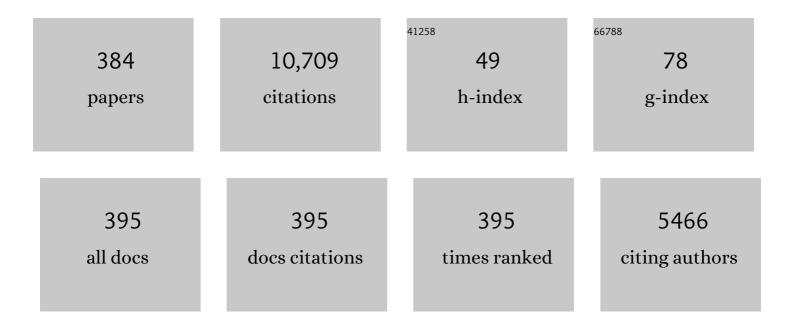
Christof Schulz

List of Publications by Year in descending order

Source: https://exaly.com/author-pdf/5688128/publications.pdf Version: 2024-02-01



#	Article	IF	CITATIONS
1	Tracer-LIF diagnostics: quantitative measurement of fuel concentration, temperature and fuel/air ratio in practical combustion systems. Progress in Energy and Combustion Science, 2005, 31, 75-121.	15.8	492
2	Laser-induced incandescence: recent trends and current questions. Applied Physics B: Lasers and Optics, 2006, 83, 333-354.	1.1	427
3	Laser-induced incandescence: Particulate diagnostics for combustion, atmospheric, and industrial applications. Progress in Energy and Combustion Science, 2015, 51, 2-48.	15.8	295
4	Modeling laser-induced incandescence of soot: a summary and comparison of LII models. Applied Physics B: Lasers and Optics, 2007, 87, 503-521.	1.1	197
5	Measurement of temperature, fuel concentration and equivalence ratio fields using tracer LIF in IC engine combustion. Applied Physics B: Lasers and Optics, 2000, 71, 717-723.	1.1	158
6	Absorption and fluorescence of toluene vapor at elevated temperatures. Physical Chemistry Chemical Physics, 2004, 6, 2940.	1.3	140
7	Autoignition of gasoline surrogates mixtures at intermediate temperatures and high pressures. Combustion and Flame, 2008, 152, 276-281.	2.8	131
8	Innovative Ultra-low NOx Controlled Auto-Ignition Combustion Process for Gasoline Engines: the 4-SPACE Project. , 0, , .		128
9	Parasitic Reactions in Nanosized Silicon Anodes for Lithium-Ion Batteries. Nano Letters, 2017, 17, 1512-1519.	4.5	122
10	Auto-ignition of toluene-doped n-heptane and iso-octane/air mixtures: High-pressure shock-tube experiments and kinetics modeling. Combustion and Flame, 2011, 158, 172-178.	2.8	118
11	Shock-tube study of the autoignition of n-heptane/toluene/air mixtures at intermediate temperatures and high pressures. Combustion and Flame, 2007, 149, 25-31.	2.8	115
12	VCSEL-based, high-speed, in situ TDLAS for in-cylinder water vapor measurements in IC engines. Optics Express, 2013, 21, 19951.	1.7	113
13	Study of the H+O+M reaction forming OHâ^—: Kinetics of OHâ^— chemiluminescence in hydrogen combustion systems. Combustion and Flame, 2010, 157, 1261-1273.	2.8	108
14	Plasma synthesis of nanostructures for improved thermoelectric properties. Journal Physics D: Applied Physics, 2011, 44, 174034.	1.3	101
15	Quantitative multi-line NO-LIF temperature imaging. Applied Physics B: Lasers and Optics, 2004, 78, 519-533.	1.1	98
16	Simultaneous single-shot laser-based imaging of formaldehyde, OH, and temperature in turbulent flames. Proceedings of the Combustion Institute, 2000, 28, 279-286.	2.4	97
17	lgnition delay times of ethanol-containing multi-component gasoline surrogates: Shock-tube experiments and detailed modeling. Fuel, 2011, 90, 1238-1244.	3.4	92
18	Gas-phase synthesis of functional nanomaterials: Challenges to kinetics, diagnostics, and process development. Proceedings of the Combustion Institute, 2019, 37, 83-108.	2.4	92

#	Article	IF	CITATIONS
19	Two-color time-resolved LII applied to soot particle sizing in the cylinder of a Diesel engine. Combustion and Flame, 2006, 147, 79-92.	2.8	91
20	SpraySyn—A standardized burner configuration for nanoparticle synthesis in spray flames. Review of Scientific Instruments, 2019, 90, 085108.	0.6	89
21	Toluene laser-induced fluorescence for in-cylinder temperature imaging in internal combustion engines. Applied Physics B: Lasers and Optics, 2008, 91, 669-675.	1.1	88
22	Autoignition of gasoline surrogate mixtures at intermediate temperatures and high pressures: Experimental and numerical approaches. Proceedings of the Combustion Institute, 2009, 32, 501-508.	2.4	84
23	Oxygen quenching of toluene fluorescence at elevated temperatures. Applied Physics B: Lasers and Optics, 2005, 80, 777-784.	1.1	81
24	Measurement and Chemical Kinetics Modeling of Shock-Induced Ignition of Ethanolâ^'Air Mixtures. Energy & Fuels, 2010, 24, 2830-2840.	2.5	80
25	Laser-induced incandescence for soot diagnostics at high pressures. Applied Optics, 2003, 42, 2052.	2.1	79
26	A direct-flame solid oxide fuel cell (DFFC) operated on methane, propane, and butane. Journal of Power Sources, 2007, 166, 120-126.	4.0	78
27	Electrical properties of aluminum-doped zinc oxide (AZO) nanoparticles synthesized by chemical vapor synthesis. Nanotechnology, 2009, 20, 445701.	1.3	77
28	Stabilization of mid-sized silicon nanoparticles by functionalization with acrylic acid. Nanoscale Research Letters, 2012, 7, 76.	3.1	74
29	Ignition delay times of diethyl ether measured in a high-pressure shock tube and a rapid compression machine. Proceedings of the Combustion Institute, 2015, 35, 259-266.	2.4	73
30	Ultraviolet absorption spectra of shock-heated carbon dioxide and water between 900 and 3050 K. Chemical Physics Letters, 2002, 355, 82-88.	1.2	72
31	Instantaneous 3D imaging of highly turbulent flames using computed tomography of chemiluminescence. Applied Optics, 2017, 56, 7385.	0.9	70
32	Strategies for laser-induced fluorescence detection of nitric oxide in high-pressure flames III Comparison of A–X excitation schemes. Applied Optics, 2003, 42, 4922.	2.1	68
33	Silicon/Polyaniline Nanocomposites as Anode Material for Lithium Ion Batteries. Journal of the Electrochemical Society, 2014, 161, A40-A45.	1.3	68
34	High-capacity cathodes for lithium-ion batteries from nanostructured LiFePO4 synthesized by highly-flexible and scalable flame spray pyrolysis. Journal of Power Sources, 2012, 216, 76-83.	4.0	66
35	Predicting LIF signal strength for toluene and 3-pentanone under engine-related temperature and pressure conditions. Proceedings of the Combustion Institute, 2005, 30, 1545-1553.	2.4	65
36	In situ nanoparticle size measurements of gas-borne silicon nanoparticles by time-resolved laser-induced incandescence. Applied Physics B: Lasers and Optics, 2014, 116, 623-636.	1.1	62

#	Article	IF	CITATIONS
37	Strategies for laser-induced fluorescence detection of nitric oxide in high-pressure flames I A–Xexcitation. Applied Optics, 2002, 41, 3547.	2.1	61
38	Combined production of power and syngas in an internal combustion engine – Experiments and simulations in SI and HCCI mode. Fuel, 2018, 215, 40-45.	3.4	61
39	Laser-induced-fluorescence detection of nitric oxide in high-pressure flames with A–X(0, 2) excitation. Applied Optics, 1997, 36, 3227.	2.1	59
40	The autoignition of practical fuels at HCCI conditions: High-pressure shock tube experiments and phenomenological modeling. Fuel, 2012, 93, 492-501.	3.4	59
41	Thermal stratification in an internal combustion engine due to wall heat transfer measured by laser-induced fluorescence. Proceedings of the Combustion Institute, 2013, 34, 2911-2919.	2.4	58
42	Direct self-assembly of Fe ₂ O ₃ /reduced graphene oxide nanocomposite for high-performance lithium-ion batteries. Journal of Materials Chemistry A, 2015, 3, 11566-11574.	5.2	58
43	Quantitative 2D single-shot imaging of no concentrations and temperatures in a transparent SI engine. Proceedings of the Combustion Institute, 1996, 26, 2597-2604.	0.3	57
44	NO-flow tagging by photodissociation of NO2. A new approach for measuring small-scale flow structures. Chemical Physics Letters, 1999, 307, 15-20.	1.2	57
45	Quantitative NO-LIF imaging in high-pressure flames. Applied Physics B: Lasers and Optics, 2002, 75, 97-102.	1.1	57
46	Toluene LIF at elevated temperatures: implications for fuel–air ratio measurements. Applied Physics B: Lasers and Optics, 2005, 80, 147-150.	1.1	57
47	Gas-Phase Synthesis of Nanoscale Silicon as an Economical Route towards Sustainable Energy Technology. KONA Powder and Particle Journal, 2011, 29, 191-207.	0.9	56
48	Enhanced coalescence upon laser desorption of fullerene oxides. Journal of Chemical Physics, 1994, 101, 3243-3249.	1.2	55
49	Simultaneous measurement of localized heat-release with OH/CH2O–LIF imaging and spatially integrated OHâ^— chemiluminescence in turbulent swirl flames. Proceedings of the Combustion Institute, 2013, 34, 3549-3556.	2.4	55
50	A quantum chemical and kinetics modeling study on the autoignition mechanism of diethyl ether. Proceedings of the Combustion Institute, 2017, 36, 195-202.	2.4	55
51	Novel strategies for imaging temperature distribution using Toluene LIF. Journal of Physics: Conference Series, 2006, 45, 133-139.	0.3	52
52	Experimental study of the kinetics of ethanol pyrolysis and oxidation behind reflected shock waves and in laminar flames. Proceedings of the Combustion Institute, 2015, 35, 393-400.	2.4	52
53	A laser-induced fluorescence scheme for imaging nitric oxide in engines. Chemical Physics Letters, 1995, 242, 259-264.	1.2	51
54	Functionalization of silicon nanoparticles via hydrosilylation with 1-alkenes. Colloid and Polymer Science, 2007, 285, 729-736.	1.0	51

#	Article	IF	CITATIONS
55	Experimental and numerical characterization of a turbulent spray flame. Proceedings of the Combustion Institute, 2007, 31, 2247-2255.	2.4	51
56	Quantitative temperature measurements in high-pressure flames with multiline NO-LIF thermometry. Applied Optics, 2005, 44, 6718.	2.1	49
57	Impact of UV absorption by CO2 and H2O on no lif inhigh-pressure combustion applications. Proceedings of the Combustion Institute, 2002, 29, 2735-2742.	2.4	48
58	High-speed tunable diode laser absorption spectroscopy for sampling-free in-cylinder water vapor concentration measurements in an optical IC engine. Applied Physics B: Lasers and Optics, 2012, 109, 521-532.	1.1	48
59	Temperature, pressure, and bath gas composition dependence of fluorescence spectra and fluorescence lifetimes of toluene and naphthalene. Applied Physics B: Lasers and Optics, 2013, 110, 81-93.	1.1	48
60	Oxygen-distribution imaging with a novel two-tracer laser-induced fluorescence technique. Applied Physics B: Lasers and Optics, 2002, 74, 111-114.	1.1	47
61	Comparison of Micro- and Nanoscale Fe+3–Containing (Hematite) Particles for Their Toxicological Properties in Human Lung Cells In Vitro. Toxicological Sciences, 2012, 126, 173-182.	1.4	47
62	Quantitative liquid and vapor distribution measurements in evaporating fuel sprays using laser-induced exciplex fluorescence. Measurement Science and Technology, 2009, 20, 125401.	1.4	46
63	Impact of shock-tube facility-dependent effects on incident- and reflected-shock conditions over a wide range of pressures and Mach numbers. Combustion and Flame, 2020, 217, 200-211.	2.8	46
64	Laser-diagnostic and numerical study of strongly swirling natural gas flames. Proceedings of the Combustion Institute, 1998, 27, 1023-1029.	0.3	45
65	Quantification of NO A–X(0, 2) laser-induced fluorescence: investigation of calibration and collisional influences in high-pressure flames. Applied Optics, 1999, 38, 1434.	2.1	45
66	Shock-tube and plug-flow reactor study of the oxidation of fuel-rich CH4/O2 mixtures enhanced with additives. Combustion and Flame, 2016, 169, 307-320.	2.8	45
67	Power and syngas production from partial oxidation of fuel-rich methane/DME mixtures in an HCCI engine. Fuel, 2019, 243, 97-103.	3.4	45
68	An experimental and modeling study on the reactivity of extremely fuel-rich methane/dimethyl ether mixtures. Combustion and Flame, 2020, 212, 107-122.	2.8	44
69	Two-line laser-induced fluorescence imaging of vibrational temperatures in a NO-seeded flame. Applied Optics, 2001, 40, 748.	2.1	43
70	Laser-induced incandescence for soot-particle sizing at elevated pressure. Applied Physics B: Lasers and Optics, 2008, 90, 629-639.	1.1	43
71	Gas-temperature imaging in a low-pressure flame reactor for nano-particle synthesis with multi-line NO-LIF thermometry. Applied Physics B: Lasers and Optics, 2007, 88, 373-377.	1.1	42
72	Influence of the bath gas on the condensation of supersaturated iron atom vapour at room temperature. Journal Physics D: Applied Physics, 2008, 41, 055203.	1.3	42

#	Article	IF	CITATIONS
73	Laser-based diagnostics in the gas-phase synthesis of inorganic nanoparticles. Powder Technology, 2016, 287, 226-238.	2.1	42
74	In-Cylinder Combustion Visualization in an Auto-Igniting Gasoline Engine using Fuel Tracer- and Formaldehyde-LIF Imaging. , 2001, , .		41
75	Initial reaction steps during flame synthesis of iron-oxide nanoparticles. CrystEngComm, 2015, 17, 6930-6939.	1.3	41
76	Two-tracer LIF imaging of preferential evaporation of multi-component gasoline fuel sprays under engine conditions. Proceedings of the Combustion Institute, 2015, 35, 2915-2922.	2.4	41
77	Sprayâ€flame synthesis of La(Fe, Co)O ₃ nanoâ€perovskites from metal nitrates. AICHE Journal, 2020, 66, e16748.	1.8	41
78	Strategies for laser-induced fluorescence detection of nitric oxide in high-pressure flames II A–X(0,1) excitation. Applied Optics, 2003, 42, 2031.	2.1	40
79	All gas-phase synthesis of graphene: Characterization and its utilization for silicon-based lithium-ion batteries. Electrochimica Acta, 2018, 272, 52-59.	2.6	40
80	Electrostatic Self-Assembly Enabling Integrated Bulk and Interfacial Sodium Storage in 3D Titania-Graphene Hybrid. Nano Letters, 2018, 18, 336-346.	4.5	40
81	Study of Soot Formation and Oxidation in the Engine Combustion Network (ECN), Spray A: Effects of Ambient Temperature and Oxygen Concentration. SAE International Journal of Engines, 0, 6, 352-365.	0.4	38
82	Combination of LII and extinction measurements for determination of soot volume fraction and estimation of soot maturity in non-premixed laminar flames. Applied Physics B: Lasers and Optics, 2015, 119, 685-696.	1.1	38
83	Two-dimensional cycle-resolved exhaust valve temperature measurements in an optically accessible internal combustion engine using thermographic phosphors. Applied Physics B: Lasers and Optics, 2012, 106, 945-951.	1.1	37
84	A Genetic Algorithmâ€Based Method for the Automatic Reduction of Reaction Mechanisms. International Journal of Chemical Kinetics, 2014, 46, 41-59.	1.0	37
85	Laser-induced incandescence from laser-heated silicon nanoparticles. Applied Physics B: Lasers and Optics, 2016, 122, 1.	1.1	37
86	Combustion Diagnostics. , 2007, , 1241-1315.		37
87	A Genetic Algorithm–Based Method for the Optimization of Reduced Kinetics Mechanisms. International Journal of Chemical Kinetics, 2015, 47, 695-723.	1.0	36
88	Laser-Based Experimental and Monte Carlo PDF Numerical Investigation of an Ethanol/Air Spray Flame. Combustion Science and Technology, 2008, 180, 1529-1547.	1.2	35
89	Imaging measurements of atomic iron concentration withÂlaser-induced fluorescence in a nanoparticle synthesis flame reactor. Applied Physics B: Lasers and Optics, 2009, 94, 119-125.	1.1	35
90	Investigation of the kinetics of OHâ^— and CHâ^— chemiluminescence in hydrocarbon oxidation behind reflected shock waves. Applied Physics B: Lasers and Optics, 2012, 107, 515-527.	1.1	34

#	Article	IF	CITATIONS
91	Determination of small soot particles in the presence of large ones from time-resolved laser-induced incandescence. Applied Physics B: Lasers and Optics, 2015, 118, 169-183.	1.1	34
92	Carbon dioxide UV laser-induced fluorescence in high-pressure flames. Chemical Physics Letters, 2003, 375, 344-349.	1.2	33
93	Quantitative in-cylinder NO-LIF imaging in a realistic gasoline engine with spray-guided direct injection. Proceedings of the Combustion Institute, 2005, 30, 2667-2674.	2.4	33
94	UV absorption of CO2 for temperature diagnostics of hydrocarbon combustion applications. Proceedings of the Combustion Institute, 2005, 30, 1591-1599.	2.4	33
95	Si–CNT/rGO Nanoheterostructures as Highâ€Performance Lithiumâ€lonâ€Battery Anodes. ChemElectroChem, 2015, 2, 1983-1990.	1.7	33
96	Temperature and species measurement in a quenching boundary layer on a flat-flame burner. Experiments in Fluids, 2010, 49, 783-795.	1.1	32
97	Shock-tube study of methane pyrolysis in the context of energy-storage processes. Proceedings of the Combustion Institute, 2019, 37, 197-204.	2.4	32
98	Measurements and simulation of in-cylinder UV-absorption in spark ignition and Diesel engines. Applied Physics B: Lasers and Optics, 2001, 73, 173-180.	1.1	31
99	Rayleigh-calibrated fluorescence quantum yield measurements of acetone and 3-pentanone. Applied Optics, 2004, 43, 5901.	2.1	31
100	Investigation of toluene LIF at high pressure and high temperature in an optical engine. Applied Physics B: Lasers and Optics, 2009, 96, 735-739.	1.1	31
101	Mechanism of Iron Oxide Formation from Iron Pentacarbonylâ€Doped Lowâ€Pressure Hydrogen/Oxygen Flames. International Journal of Chemical Kinetics, 2013, 45, 487-498.	1.0	31
102	Gas-phase synthesis of iron oxide nanoparticles for improved magnetic hyperthermia performance. Journal of Alloys and Compounds, 2020, 824, 153814.	2.8	31
103	Flexible energy conversion and storage via high-temperature gas-phase reactions: The piston engine as a polygeneration reactor. Renewable and Sustainable Energy Reviews, 2020, 133, 110264.	8.2	31
104	TR-LII for sizing of carbon particles forming at room temperature. Applied Physics B: Lasers and Optics, 2006, 83, 449-454.	1.1	30
105	Measurement of water film thickness by laser-induced fluorescence and Raman imaging. Applied Physics B: Lasers and Optics, 2011, 102, 123-132.	1.1	30
106	Temperature and bath gas composition dependence of effective fluorescence lifetimes of toluene excited at 266nm. Chemical Physics, 2011, 383, 6-11.	0.9	30
107	A shock tube with a high-repetition-rate time-of-flight mass spectrometer for investigations of complex reaction systems. Review of Scientific Instruments, 2011, 82, 084103.	0.6	30
108	Photo-physical properties of anisole: temperature, pressure, and bath gas composition dependence of fluorescence spectra and lifetimes. Applied Physics B: Lasers and Optics, 2013, 112, 203-213.	1.1	30

#	Article	IF	CITATIONS
109	Surface functionalization of microwave plasma-synthesized silica nanoparticles for enhancing the stability of dispersions. Journal of Nanoparticle Research, 2014, 16, 1.	0.8	30
110	Laser diagnostic analysis of no formation in a direct injection diesel engine with pump-line-nozzle and common rail injection systems. Proceedings of the Combustion Institute, 2000, 28, 1137-1143.	2.4	29
111	Single-shot laser-induced fluorescence imaging of formaldehyde with XeF excimer excitation. Applied Physics B: Lasers and Optics, 2000, 70, 733-735.	1.1	29
112	A comparison of selected organic tracers for quantitative scalar imaging in the gas phase via laser-induced fluorescence. Applied Physics B: Lasers and Optics, 2014, 117, 183-194.	1.1	29
113	Laser-based in situ measurement and simulation of gas-phase temperature and iron atom concentration in a pilot-plant nanoparticle synthesis reactor. Proceedings of the Combustion Institute, 2015, 35, 2299-2306.	2.4	29
114	Towards Mechanistic Understanding of Liquidâ€Phase Cinnamyl Alcohol Oxidation with tert â€Butyl Hydroperoxide over Nobleâ€Metalâ€Free LaCo 1– x Fe x O 3 Perovskites. ChemPlusChem, 2019, 84, 1155-1163	1.3	29
115	Durability study of platinum nanoparticles supported on gas-phase synthesized graphene in oxygen reduction reaction conditions. Applied Surface Science, 2019, 467-468, 1181-1186.	3.1	29
116	Large-scale synthesis of iron oxide/graphene hybrid materials as highly efficient photo-Fenton catalyst for water remediation. Environmental Technology and Innovation, 2021, 21, 101239.	3.0	29
117	Simultaneous measurement of localized heat release with OH/CH2O-LIF imaging and spatially integrated OHâ^— chemiluminescence in turbulent swirl flames. Applied Physics B: Lasers and Optics, 2012, 107, 611-617.	1.1	28
118	Autoignition of surrogate biodiesel fuel (B30) at high pressures: Experimental and modeling kinetic study. Combustion and Flame, 2012, 159, 996-1008.	2.8	28
119	Sprayâ€Flameâ€Synthesized LaCo 1â^' x Fe x O 3 Perovskite Nanoparticles as Electrocatalysts for Water and Ethanol Oxidation. ChemElectroChem, 2019, 6, 4266-4274.	1.7	28
120	Selective cyclohexene oxidation with O ₂ , H ₂ O ₂ and <i>tert</i> -butyl hydroperoxide over spray-flame synthesized LaCo _{1â[°]x} Fe _x O ₃ nanoparticles. Catalysis Science and Technology, 2020, 10, 5196-5206.	2.1	28
121	Development of a two-line OH-laser-induced fluorescence thermometry diagnostics strategy for gas-phase temperature measurements in engines. Applied Optics, 2008, 47, 5871.	2.1	27
122	Experiments and modeling of ignition delay times, flame structure and intermediate species of EHN-doped stoichiometric n-heptane/air combustion. Proceedings of the Combustion Institute, 2009, 32, 197-204.	2.4	27
123	Experimental and Numerical Investigation of Fe(CO) ₅ Addition to a Laminar Premixed Hydrogen/Oxygen/Argon Flame. Zeitschrift Fur Physikalische Chemie, 2009, 223, 639-649.	1.4	27
124	An automated thermophoretic soot sampling device for laboratory-scale high-pressure flames. Review of Scientific Instruments, 2014, 85, 045103.	0.6	27
125	A novel magnetically-separable porous iron-oxide nanocomposite as an adsorbent for methylene blue (MB) dye. Journal of Environmental Chemical Engineering, 2016, 4, 3779-3787.	3.3	27
126	Experimental and numerical study of a HMDSO-seeded premixed laminar low-pressure flame for SiO2 nanoparticle synthesis. Proceedings of the Combustion Institute, 2017, 36, 1045-1053.	2.4	27

#	Article	IF	CITATIONS
127	Optical properties and pyrolysis of shock-heated gas-phase anisole. Proceedings of the Combustion Institute, 2017, 36, 4525-4532.	2.4	27
128	Synthesis of freestanding few-layer graphene in microwave plasma: The role of oxygen. Carbon, 2022, 186, 560-573.	5.4	27
129	Simultaneous Mapping of the Distribution of Different Fuel Volatility Classes Using Tracer-LIF Tomography in an IC Engine. , 1998, , .		26
130	Quantitative oxygen imaging in an engine. Applied Physics B: Lasers and Optics, 2002, 75, 137-141.	1.1	26
131	Vibrational and defect states in SnOx nanoparticles. Journal of Applied Physics, 2006, 99, 113108.	1.1	26
132	Heat release of carbon particle formation from hydrogen-free precursors behind shock waves. Proceedings of the Combustion Institute, 2007, 31, 649-656.	2.4	26
133	Unsteady flame and flow field interaction of a premixed model gas turbine burner. Proceedings of the Combustion Institute, 2007, 31, 3197-3205.	2.4	26
134	Sensitivity analysis for soot particle size imaging with laser-induced incandescence at high pressure. Applied Physics B: Lasers and Optics, 2015, 119, 745-763.	1.1	26
135	Detailed modeling and laser-induced fluorescence imaging of nitric oxide in a NH3-seeded non-premixed methane/air flame. Proceedings of the Combustion Institute, 2002, 29, 2195-2202.	2.4	25
136	Gas-phase temperature imaging in spray systems using multi-line NO-LIF thermometry. Applied Physics B: Lasers and Optics, 2005, 81, 1071-1074.	1.1	25
137	Modeling laser-induced incandescence of soot: enthalpy changes during sublimation, conduction, and oxidation. Applied Physics B: Lasers and Optics, 2008, 93, 645-656.	1.1	25
138	Simultaneous measurement of liquid water film thickness andÂvapor temperature using near-infrared tunable diode laser spectroscopy. Applied Physics B: Lasers and Optics, 2010, 99, 385-390.	1.1	25
139	Quantitative two-dimensional measurement of oil-film thickness by laser-induced fluorescence in a piston-ring model experiment. Applied Optics, 2016, 55, 269.	2.1	25
140	Synthesis of silicon nanoparticles in a pilot-plant-scale microwave plasma reactor: Impact of flow rates and precursor concentration on the nanoparticle size and aggregation. Powder Technology, 2019, 342, 880-886.	2.1	25
141	Room-temperature Fe:ZnSe laser tunable in the spectral range of 3.7–5.3â€Âµm applied for intracavity absorption spectroscopy of CO ₂ isotopes, CO and N ₂ O. Optics Express, 2021, 29, 12033.	1.7	25
142	Advanced direct injection combustion engine technologies and development. , 2010, , .		25
143	Investigation of spatially resolved light absorption in a spark-ignition engine fueled with propane/air. Applied Optics, 1999, 38, 1452.	2.1	24
144	Branching ratios for quenching of nitric oxide A2Σ+(ν′ = 0) to X2Î(ν″ = 0). Physical Chemistry Chemical Physics, 2006, 8, 5328-5338.	1.3	24

#	Article	IF	CITATIONS
145	Direct-Flame Solid-Oxide Fuel Cell (DFFC): A Thermally Self-Sustained, Air Self- Breathing, Hydrocarbon-Operated SOFC System in a Simple, No-Chamber Setup. ECS Transactions, 2007, 7, 555-564.	0.3	24
146	Spectroscopic characterization of the fluorobenzene/DEMA tracer system for laser-induced exciplex fluorescence for the quantitative study of evaporating fuel sprays. Applied Physics B: Lasers and Optics, 2009, 97, 909-918.	1.1	24
147	Visualization of the evaporation of a diesel spray using combined Mie and Rayleigh scattering techniques. Experiments in Fluids, 2009, 47, 439-449.	1.1	24
148	Unburned gas temperature measurements in a surrogate Diesel jet via two-color toluene-LIF imaging. Proceedings of the Combustion Institute, 2011, 33, 783-790.	2.4	24
149	Impact of Ambient Pressure on Titania Nanoparticle Formation During Spray-Flame Synthesis. Journal of Nanoscience and Nanotechnology, 2015, 15, 9449-9456.	0.9	24
150	Ignition delay times of Jet A-1 fuel: Measurements in a high-pressure shock tube and a rapid compression machine. Proceedings of the Combustion Institute, 2017, 36, 3695-3703.	2.4	24
151	Soot formation in shock-wave-induced pyrolysis of acetylene and benzene with H2, O2, and CH4 addition. Combustion and Flame, 2018, 198, 158-168.	2.8	24
152	Two-Dimensional Temperature Measurements in an SI Engine Using Two-Line Tracer LIF. , 0, , .		23
153	Imaging of the oxygen distribution in an isothermal turbulent free jet using two-color toluene LIF imaging. Applied Physics B: Lasers and Optics, 2011, 103, 707-715.	1.1	23
154	Tunable diode laser absorption sensor for the simultaneous measurement of water film thickness, liquid- and vapor-phase temperature. Applied Physics B: Lasers and Optics, 2011, 104, 21-27.	1.1	23
155	A single-pulse shock tube coupled with high-repetition-rate time-of-flight mass spectrometry and gas chromatography for high-temperature gas-phase kinetics studies. Review of Scientific Instruments, 2016, 87, 105103.	0.6	23
156	Shock-tube study of the ignition and product formation of fuel-rich CH4/air and CH4/additive/air mixtures at high pressure. Proceedings of the Combustion Institute, 2019, 37, 5705-5713.	2.4	23
157	Characterization of tracers for two-color laser-induced fluorescence liquid-phase temperature imaging in sprays. Experiments in Fluids, 2020, 61, 1.	1.1	23
158	Time-resolved detection of temperature, concentration, and pressure in a shock tube by intracavity absorption spectroscopy. Applied Physics B: Lasers and Optics, 2016, 122, 1.	1.1	22
159	Comparative study of flame-based SiO2 nanoparticle synthesis from TMS and HMDSO: SiO-LIF concentration measurement and detailed simulation. Proceedings of the Combustion Institute, 2019, 37, 1221-1229.	2.4	22
160	Discrepancies between shock tube and rapid compression machine ignition at low temperatures and high pressures. , 2009, , 739-744.		22
161	Core and grain boundary sensitivity of tungsten-oxide sensor devices by molecular beam assisted particle deposition. Journal of Applied Physics, 2007, 102, 124305.	1.1	21
162	Synthesis of SnO2â^'x nanoparticles tuned between 0⩽x⩽1 in a premixed low pressure H2/O2/Ar flame. Proceedings of the Combustion Institute, 2007, 31, 1805-1812.	2.4	21

#	Article	IF	CITATIONS
163	Synthesis of tailored WO3 and WOx (2.9 <x<3) 1883-1890.<="" 2011,="" 33,="" a="" adjusting="" ar="" by="" combustion="" conditions="" flame="" h2="" in="" institute,="" nanoparticles="" o2="" of="" premixed="" proceedings="" reactor.="" td="" the=""><td>2.4</td><td>21</td></x<3)>	2.4	21
164	Calibration-free, high-speed, in-cylinder laser absorption sensor for cycle-resolved, absolute H2O measurements in a production IC engine. Proceedings of the Combustion Institute, 2015, 35, 3653-3661.	2.4	21
165	Assessment of soot particle-size imaging with LII at Diesel engine conditions. Applied Physics B: Lasers and Optics, 2015, 119, 765-776.	1.1	21
166	Spectroscopic models for laser-heated silicon and copper nanoparticles. Journal of Quantitative Spectroscopy and Radiative Transfer, 2017, 197, 3-11.	1.1	21
167	Direct Measurement of High-Temperature Rate Constants of the Thermal Decomposition of Dimethoxymethane, a Shock Tube and Modeling Study. Journal of Physical Chemistry A, 2018, 122, 7559-7571.	1.1	21
168	Sprayâ€Flameâ€Prepared LaCo _{1–<i>x</i>} Fe _x O ₃ Perovskite Nanoparticles as Active OER Catalysts: Influence of Fe Content and Lowâ€Temperature Heating. ChemElectroChem, 2020, 7, 2564-2574.	1.7	21
169	Plug-flow reactor and shock-tube study of the oxidation of very fuel-rich natural gas/DME/O2 mixtures. Combustion and Flame, 2021, 225, 86-103.	2.8	21
170	Laser-induced incandescence for non-soot nanoparticles: recent trends and current challenges. Applied Physics B: Lasers and Optics, 2022, 128, 72.	1.1	21
171	Laser-induced fluorescence of tracers dissolved in evaporating droplets. Applied Physics B: Lasers and Optics, 2004, 78, 127-131.	1.1	20
172	Endoscopic temperature imaging in a four-cylinder IC engine via two-color toluene fluorescence. Proceedings of the Combustion Institute, 2015, 35, 3697-3705.	2.4	20
173	Measurements of liquid film thickness, concentration, and temperature of aqueous urea solution by NIR absorption spectroscopy. Applied Physics B: Lasers and Optics, 2016, 122, 1.	1.1	20
174	Detailed simulation of iron oxide nanoparticle forming flames: Buoyancy and probe effects. Proceedings of the Combustion Institute, 2019, 37, 1241-1248.	2.4	20
175	Characterization of few-layer graphene aerosols by laser-induced incandescence. Carbon, 2020, 167, 870-880.	5.4	20
176	Experimental and numerical investigation of iron-doped flames: FeO formation and impact on flame temperature. Proceedings of the Combustion Institute, 2021, 38, 1249-1257.	2.4	20
177	Laser Diagnostics of Combustion Processes: From Chemical Dynamics to Technical Devices. Israel Journal of Chemistry, 1999, 39, 1-24.	1.0	19
178	Laser-diagnostic multi-species imaging in strongly swirling natural gas flames. Applied Physics B: Lasers and Optics, 2000, 71, 741-746.	1.1	19
179	Numerical simulation and laser-based imaging of mixture formation, ignition, and soot formation in a diesel spray. Proceedings of the Combustion Institute, 2005, 30, 2029-2036.	2.4	19
180	Endoscopic Imaging of Early Flame Propagation in a Near-Production Engine. SAE International Journal of Engines, 0, 7, 351-365.	0.4	19

#	Article	IF	CITATIONS
181	High-pressure shock-tube study of the ignition and product formation of fuel-rich dimethoxymethane (DMM)/air and CH4/DMM/air mixtures. Combustion and Flame, 2020, 216, 293-299.	2.8	19
182	Spray-flame synthesis of LaMO3 (M = Mn, Fe, Co) perovskite nanomaterials: Effect of spray droplet size and esterification on particle size distribution. Proceedings of the Combustion Institute, 2021, 38, 1279-1287.	2.4	19
183	Laser-induced atomic emission of silicon nanoparticles during laser-induced heating. Applied Optics, 2017, 56, E50.	2.1	19
184	Laser Spectroscopic Investigation of Flow Fields and NO-Formation in a Realistic SI Engine. , 1998, , .		18
185	Nonstationary Collisional Dynamics in Determining Nitric Oxide Laser-Induced Flourescence Spectra. AIAA Journal, 2005, 43, 458-464.	1.5	18
186	Three-dimensional modeling with Monte Carlo-probability density function methods and laser diagnostics of the combustion in a two-stroke engine. Proceedings of the Combustion Institute, 2000, 28, 1153-1159.	2.4	17
187	Fluorescence lifetime of gas-phase toluene at elevated temperatures. Chemical Physics Letters, 2006, 426, 248-251.	1.2	17
188	Thermal Decomposition of Trimethylgallium Ga(CH ₃) ₃ : A Shock-Tube Study and First-Principles Calculations. Journal of Physical Chemistry A, 2008, 112, 6330-6337.	1.1	17
189	Laser-based diagnostics for the measurement of liquid water film thickness. Applied Optics, 2011, 50, A60.	2.1	17
190	Mass spectrometric analysis of clusters and nanoparticles during the gas-phase synthesis of tungsten oxide. Proceedings of the Combustion Institute, 2017, 36, 1037-1044.	2.4	17
191	SiO multi-line laser-induced fluorescence for quantitative temperature imaging in flame-synthesis of nanoparticles. Applied Physics B: Lasers and Optics, 2017, 123, 1.	1.1	16
192	LIISim: a modular signal processing toolbox for laser-induced incandescence measurements. Applied Physics B: Lasers and Optics, 2018, 124, 1.	1.1	16
193	Highâ€Temperature Rate Constants for H + Tetramethylsilane and H + Silane and Implications about Structure–Activity Relationships for Silanes. International Journal of Chemical Kinetics, 2018, 50, 57-72.	1.0	16
194	Response surface and group additivity methodology for estimation of thermodynamic properties of organosilanes. International Journal of Chemical Kinetics, 2018, 50, 681-690.	1.0	16
195	Development and evaluation of a chemical kinetics reaction mechanism for tetramethylsilane-doped flames. Chemical Engineering Science, 2019, 209, 115209.	1.9	16
196	Self-assembled nano-silicon/graphite hybrid embedded in a conductive polyaniline matrix for the performance enhancement of industrial applicable lithium-ion battery anodes. Solid State Ionics, 2020, 344, 115117.	1.3	16
197	Laser-based CO concentration and temperature measurements in high-pressure shock-tube studies of n-heptane partial oxidation. Applied Physics B: Lasers and Optics, 2020, 126, 1.	1.1	16
198	CO-concentration and temperature measurements in reacting CH4/O2 mixtures doped with diethyl ether behind reflected shock waves. Combustion and Flame, 2020, 216, 194-205.	2.8	16

#	Article	IF	CITATIONS
199	Atmospheric-pressure particle mass spectrometer for investigating particle growth in spray flames. Journal of Aerosol Science, 2021, 158, 105827.	1.8	16
200	Multidimensional laser diagnostic and numerical analysis of no formation in a gasoline engine. Proceedings of the Combustion Institute, 1998, 27, 2085-2092.	0.3	15
201	Multi-Species Laser-Based Imaging Measurements in a Diesel Spray. , 0, , .		15
202	Buoyancy induced limits for nanoparticle synthesis experiments in horizontal premixed low-pressure flat-flame reactors. Combustion Theory and Modelling, 2013, 17, 504-521.	1.0	15
203	Influence of molecular hydrogen on acetylene pyrolysis: Experiment and modeling. Combustion and Flame, 2014, 161, 2263-2269.	2.8	15
204	Measurements of liquid film thickness, concentration and temperature of aqueous NaCl solution by NIR absorption spectroscopy. Applied Physics B: Lasers and Optics, 2015, 120, 397-406.	1.1	15
205	High-yield and scalable synthesis of a Silicon/Aminosilane-functionalized Carbon NanoTubes/Carbon (Si/A-CNT/C) composite as a high-capacity anode for lithium-ion batteries. Journal of Applied Electrochemistry, 2016, 46, 229-239.	1.5	15
206	A Shock Tube and Modeling Study about Anisole Pyrolysis Using Time-Resolved CO Absorption Measurements. International Journal of Chemical Kinetics, 2017, 49, 656-667.	1.0	15
207	Flame-temperature, light-attenuation, and CO measurements by spontaneous Raman scattering in non-sooting diesel-like jets. Combustion and Flame, 2017, 176, 104-116.	2.8	15
208	Water film thickness imaging based on time-multiplexed near-infrared absorption. Optics Express, 2018, 26, 20902.	1.7	15
209	Diffractive/refractive (hybrid) UV-imaging system for minimally invasive metrology: design, performance, and application experiments. Applied Optics, 2012, 51, 1982.	0.9	14
210	Nanoparticles from the Gasphase. Nanoscience and Technology, 2012, , .	1.5	14
211	High-pressure shock-tube investigation of the impact of 3-pentanone on the ignition properties of primary reference fuels. Proceedings of the Combustion Institute, 2013, 34, 393-400.	2.4	14
212	Temporally and spectrally resolved UV absorption and laser-induced fluorescence measurements during the pyrolysis of toluene behind reflected shock waves. Applied Physics B: Lasers and Optics, 2015, 118, 295-307.	1.1	14
213	Two-dimensional-three-dimensional registration for fusion imaging is noninferior to three-dimensional- three-dimensional registration in infrarenal endovascular aneurysm repair. Journal of Vascular Surgery, 2019, 70, 2005-2013.	0.6	14
214	Ethanol ignition in a high-pressure shock tube: Ignition delay time and high-repetition-rate imaging measurements. Proceedings of the Combustion Institute, 2021, 38, 901-909.	2.4	14
215	Experimental Investigation of Ethanol Oxidation and Development of a Reduced Reaction Mechanism for a Wide Temperature Range. Energy & amp; Fuels, 2021, 35, 14780-14792.	2.5	14
216	Comparative study of experimental and numerical no profiles in SI combustion. Proceedings of the Combustion Institute, 1998, 27, 2077-2084.	0.3	13

#	Article	IF	CITATIONS
217	In-Cylinder NO-LIF Imaging in a Realistic GDI Engine Using KrF Excimer Laser Excitation. , 1999, , .		13
218	Gas-phase synthesis of non-agglomerated nanoparticles by fast gasdynamic heating and cooling. , 2009, , 857-862.		13
219	A Standard Burner for High Pressure Laminar Premixed Flames: Detailed Soot Diagnostics. Zeitschrift Fur Physikalische Chemie, 2015, 229, 781-805.	1.4	13
220	Shock-tube study of the decomposition of tetramethylsilane using gas chromatography and high-repetition-rate time-of-flight mass spectrometry. Physical Chemistry Chemical Physics, 2018, 20, 10686-10696.	1.3	13
221	Investigating temporal variation in the apparent volume fraction measured by time-resolved laser-induced incandescence. Applied Physics B: Lasers and Optics, 2019, 125, 1.	1.1	13
222	Inline coating of silicon nanoparticles in a plasma reactor: Reactor design, simulation and experiment. Materials Today: Proceedings, 2017, 4, S118-S127.	0.9	13
223	Quantitative Laser Diagnostic Studies of the NO Distribution in a DI Diesel Engine with PLN and CR Injection Systems. , 0, , .		12
224	Spray diagnostics using an all-solid-state Nd:YAlO3 laser and fluorescence tracers in commercial gasoline and diesel fuels. Applied Physics B: Lasers and Optics, 2004, 79, 249-254.	1.1	12
225	Quantification of the evaporative cooling in an ethanol spray created by a gasoline direct-injection system measured by multiline NO-LIF gas-temperature imaging. Applied Optics, 2007, 46, 8322.	2.1	12
226	Gas-Temperature Imaging in aÂMicrowave-Plasma Nanoparticle-Synthesis Reactor Using Multi-Line NO-LIF Thermometry. Zeitschrift Fur Physikalische Chemie, 2011, 225, 1225-1235.	1.4	12
227	Experimental and modeling study of carbon suboxide decomposition behind reflected shock waves. Physical Chemistry Chemical Physics, 2012, 14, 1246-1252.	1.3	12
228	Low-pressure effective fluorescence lifetimes and photo-physical rate constants of one- and two-ring aromatics. Applied Physics B: Lasers and Optics, 2015, 121, 549-558.	1.1	12
229	Performance of photomultipliers in the context of laser-induced incandescence. Applied Optics, 2017, 56, 7849.	0.9	12
230	Sequential signal detection for high dynamic range time-resolved laser-induced incandescence. Optics Express, 2017, 25, 2413.	1.7	12
231	The influence of hydrogen and methane on the growth of carbon particles during acetylene pyrolysis in a burnt-gas flow reactor. Proceedings of the Combustion Institute, 2019, 37, 1125-1132.	2.4	12
232	High-Temperature Unimolecular Decomposition of Diethyl Ether: Shock-Tube and Theory Studies. Journal of Physical Chemistry A, 2019, 123, 6813-6827.	1.1	12
233	Absolute SiO concentration imaging in low-pressure nanoparticle-synthesis flames via laser-induced fluorescence. Applied Physics B: Lasers and Optics, 2019, 125, 1.	1.1	12
234	Detector calibration and measurement issues in multi-color time-resolved laser-induced incandescence. Applied Physics B: Lasers and Optics, 2019, 125, 1.	1.1	12

#	Article	IF	CITATIONS
235	Multi-line SiO fluorescence imaging in the flame synthesis of silica nanoparticles from SiCl4. Combustion and Flame, 2021, 224, 260-272.	2.8	12
236	Formation of carbon nanoparticles by the condensation of supersaturated atomic vapor obtained by the laser photolysis of C3O2. Kinetics and Catalysis, 2007, 48, 194-203.	0.3	11
237	Self-quenching in toluene LIF. Proceedings of the Combustion Institute, 2017, 36, 4505-4514.	2.4	11
238	Quantitative nitrogen oxide measurements by laser-induced fluorescence in diesel-like n-heptane jets with enhanced premixing. Combustion and Flame, 2018, 188, 250-261.	2.8	11
239	A six-compound, high performance gasoline surrogate for internal combustion engines: Experimental and numerical study of autoignition using high-pressure shock tubes. Fuel, 2020, 261, 116439.	3.4	11
240	Monitoring formaldehyde in a shock tube with a fast dual-comb spectrometer operating in the spectral range of 1740–1790Âcm–1. Applied Physics B: Lasers and Optics, 2020, 126, 1.	1.1	11
241	Characterization of tracers for two-color laser-induced fluorescence thermometry of liquid-phase temperature in ethanol, 2–ethylhexanoic-acid/ethanol mixtures, 1-butanol, and o-xylene. Applied Optics, 2021, 60, C98.	0.9	11
242	A Cr ⁴⁺ :forsterite laser for intracavity absorption spectroscopy in the spectral range of 12–14 Âμm. Optics Express, 2019, 27, 11122.	1.7	11
243	LES of nanoparticle synthesis in the spraysyn burner: A comparison against experiments. Powder Technology, 2022, 404, 117466.	2.1	11
244	Fluorescence imaging of natural gas/air mixing without tracers added. Chemical Physics Letters, 2001, 345, 259-264.	1.2	10
245	UV planar laser induced fluorescence imaging of hot carbon dioxide in a high-pressure flame. Applied Physics B: Lasers and Optics, 2004, 79, 427-430.	1.1	10
246	Effects of Bio Diesel Injection in a DI Diesel Engine on Gaseous and Particulate Emission. , 2005, , .		10
247	Experimental investigation and modeling of the kinetics of CCl4 pyrolysis behind reflected shock waves using high-repetition-rate time-of-flight mass spectrometry. Physical Chemistry Chemical Physics, 2013, 15, 2821.	1.3	10
248	Nitric Oxide Measurements in the Core of Diesel Jets Using a Biofuel Blend. SAE International Journal of Materials and Manufacturing, 2015, 8, 458-471.	0.3	10
249	Effect of fluctuations on time-averaged multi-line NO-LIF thermometry measurements of the gas-phase temperature. Applied Physics B: Lasers and Optics, 2015, 120, 429-440.	1.1	10
250	Micrometer-sized nano-structured silicon/carbon composites for lithium-ion battery anodes synthesized based on a three-step Hansen solubility parameter (HSP) concept. Journal of Industrial and Engineering Chemistry, 2017, 52, 305-313.	2.9	10
251	High-temperature gas-phase kinetics of the thermal decomposition of tetramethoxysilane. Proceedings of the Combustion Institute, 2019, 37, 1133-1141.	2.4	10
252	Laser spectroscopic investigation of diesel-like jet structure using C8 oxygenates as the fuel. Fuel, 2019, 235, 1515-1529.	3.4	10

#	Article	IF	CITATIONS
253	Pyrolysis of diethyl carbonate: Shock-tube and flow-reactor measurements and modeling. Proceedings of the Combustion Institute, 2021, 38, 987-996.	2.4	10
254	Spatial distribution of gas-phase synthesized germanium nanoparticle volume-fraction and temperature using combined in situ line-of-sight emission and extinction spectroscopy. Optics Express, 2021, 29, 8387.	1.7	10
255	Interrogating Gas-Borne Nanoparticles Using Laser-Based Diagnostics and Bayesian Data Fusion. Journal of Physical Chemistry C, 2021, 125, 8382-8390.	1.5	10
256	Liquidâ€Phase Cyclohexene Oxidation with O ₂ over Sprayâ€Flameâ€Synthesized La _{1â^'<i>x</i>} Sr _{<i>x</i>} CoO ₃ Perovskite Nanoparticles. Chemistry - A European Journal, 2021, 27, 16912-16923.	1.7	10
257	Laser-spectroscopic investigation of OH-radical concentrations in the exhaust plane of jet engines. Geophysical Research Letters, 1999, 26, 1849-1852.	1.5	9
258	Fluorescence quantum yield of carbon dioxide for quantitative UV laser-induced fluorescence in high-pressure flames. Applied Physics B: Lasers and Optics, 2008, 93, 677-685.	1.1	9
259	Influence of carbon content, particle size, and partial manganese substitution on the electrochemical performance of LiFexMn1-xPO4/carbon composites. Ionics, 2015, 21, 1857-1866.	1.2	9
260	Investigation of the combustion of iron pentacarbonyl and the formation of key intermediates in iron oxide synthesis flames. Chemical Engineering Science, 2021, 230, 116169.	1.9	9
261	Crumpled few-layer graphene: Connection between morphology and optical properties. Carbon, 2021, 182, 677-690.	5.4	9
262	Near-threshold soot formation in premixed flames at elevated pressure. Carbon, 2021, 181, 143-154.	5.4	9
263	Investigating spray flames for nanoparticle synthesis via tomographic imaging using multi-simultaneous measurements (TIMes) of emission. Optics Express, 2022, 30, 15524.	1.7	9
264	Quantitative In-Cylinder NO-LIF Imaging in a Direct-Injected Gasoline Engine with Exhaust Gas Recirculation. , 2001, , .		8
265	Mixing Processes in a Compressible Accelerated Nozzle Flow with Blunt-Body Wakes. AIAA Journal, 2014, 52, 559-568.	1.5	8
266	Diode laser-based standoff absorption measurement of water film thickness in retro-reflection. Applied Physics B: Lasers and Optics, 2016, 122, 1.	1.1	8
267	UV absorption and fluorescence properties of gas-phase p-difluorobenzene. Applied Physics B: Lasers and Optics, 2017, 123, 1.	1.1	8
268	Novel Si-CNT/polyaniline nanocomposites as Lithium-ion battery anodes for improved cycling performance. Materials Today: Proceedings, 2017, 4, S263-S268.	0.9	8
269	High-Temperature Rate Constants for the Reaction of Hydrogen Atoms with Tetramethoxysilane and Reactivity Analogies between Silanes and Oxygenated Hydrocarbons. Journal of Physical Chemistry A, 2018, 122, 5289-5298.	1.1	8
270	Determination of gas-phase absorption cross-sections of FeO in a shock tube using intracavity absorption spectroscopy near 611†nm. Proceedings of the Combustion Institute, 2021, 38, 1637-1645.	2.4	8

#	Article	IF	CITATIONS
271	Early particle formation and evolution in iron-doped flames. Combustion and Flame, 2022, 244, 112251.	2.8	8
272	Instantaneous three-dimensional visualization of concentration distributions in turbulent flows with crossed-plane laser-induced fluorescence imaging. Applied Physics B: Lasers and Optics, 2005, 80, 125-131.	1.1	7
273	Laser-based temperature imaging close to surfaces with toluene and NO-LIF. Journal of Physics: Conference Series, 2006, 45, 69-76.	0.3	7
274	Probing Species Formed by Pilot Injection During Re-Compression in a Controlled Auto-Ignition Engine by H2CO LIF and Chemiluminescence Imaging. SAE International Journal of Engines, 2014, 7, 772-789.	0.4	7
275	Optical Investigation of Biofuel Effects on NO and PAH Formation in Diesel-Like Jets. , 2015, , .		7
276	A group additivity methodology for predicting the thermochemistry of oxygen ontaining organosilanes. International Journal of Chemical Kinetics, 2020, 52, 918-932.	1.0	7
277	Numerical Investigation of Remote Ignition in Shock Tubes. Flow, Turbulence and Combustion, 2021, 106, 471-498.	1.4	7
278	Temperature and Heat Flux. , 2007, , 487-561.		7
279	NIR sensor for aqueous urea solution film thickness and concentration measurement using a broadband light source. Applied Optics, 2019, 58, 4546.	0.9	7
280	Method for absolute OH-concentration measurements in premixed flames by LIF and numerical simulations. Applied Physics B: Lasers and Optics, 2004, 79, 759-766.	1.1	6
281	Nanoparticle formation from supersaturated carbon vapour generated by laser photolysis of carbon suboxide. Journal Physics D: Applied Physics, 2006, 39, 4359-4365.	1.3	6
282	Ga2O3 nanoparticles synthesized in a low-pressure flame reactor. Journal of Nanoparticle Research, 2008, 10, 121-127.	0.8	6
283	High temperature shock-tube study of the reaction of gallium with ammonia. Physical Chemistry Chemical Physics, 2011, 13, 4149.	1.3	6
284	Strain rate and fuel composition dependence of chemiluminescent species profiles in non-premixed counterflow flames: comparison with model results. Applied Physics B: Lasers and Optics, 2012, 107, 561-569.	1.1	6
285	Mixture-Formation Analysis by PLIF in an HSDI Diesel Engine Using C ₈ -Oxygenates as the Fuel. SAE International Journal of Fuels and Lubricants, 0, 8, 396-414.	0.2	6
286	Reaction-time-resolved measurements of laser-induced fluorescence in a shock tube with a single laser pulse. Review of Scientific Instruments, 2017, 88, 115105.	0.6	6
287	Application of toluene LIF to transonic nozzle flows to identify zones of incomplete molecular mixing. Optics Express, 2018, 26, 10266.	1.7	6
288	Thermochemistry of organosilane compounds and organosilyl radicals. Proceedings of the Combustion Institute, 2021, 38, 1259-1267.	2.4	6

#	Article	IF	CITATIONS
289	Phase-sensitive detection of gas-borne Si nanoparticles via line-of-sight UV/VIS attenuation. Optics Express, 2021, 29, 21795.	1.7	6
290	Uncertainty quantification and design-of-experiment in absorption-based aqueous film parameter measurements using Bayesian inference. Applied Optics, 2017, 56, E1.	2.1	6
291	Shock-tube study of the decomposition of octamethylcyclotetrasiloxane and hexamethylcyclotrisiloxane. Zeitschrift Fur Physikalische Chemie, 2020, 234, 1395-1426.	1.4	6
292	In situ measurement of gas-borne silicon nanoparticle volume fraction and temperature by spatially and spectrally line-resolved attenuation and emission imaging. Powder Technology, 2022, 396, 535-541.	2.1	6
293	Measurement of the Equivalence Ratio in the Spark Gap Region of a Gasoline Direct Injection Engine With Spark Emission Spectroscopy and Tracer-LIF. , 2004, , .		5
294	Advanced Laser Imaging Diagnostics in Combustion. Zeitschrift Fur Physikalische Chemie, 2005, 219, 509-554.	1.4	5
295	Toluene Laser-Induced Fluorescence (LIF) Under Engine-Related Pressures, Temperatures and Oxygen Mole Fractions. , 2005, , .		5
296	Laser-Induced Incandescence. Applied Physics B: Lasers and Optics, 2006, 83, 331-331.	1.1	5
297	Hybrid Endoscopes for Laser-Based Imaging Diagnostics in IC Engines. , 0, , .		5
298	In-cylinder temperature measurements via time-correlated single-photon counting of toluene laser-induced fluorescence through a fiber-based sensor. Optics Letters, 2012, 37, 5244.	1.7	5
299	Synthesis of Small Carbon Nanoparticles in a Microwave Plasma Flow Reactor. Zeitschrift Fur Physikalische Chemie, 2013, 227, 357-370.	1.4	5
300	Formaldehyde laser-induced fluorescence imaging with a multi-band transmission filter. Optics Letters, 2014, 39, 1873.	1.7	5
301	lgnition delay times of shock-heated tetraethoxysilane, hexamethyldisiloxane, and titanium tetraisopropoxide. Chemical Physics Letters, 2014, 601, 54-58.	1.2	5
302	Endoscopic Chemiluminescence Measurements as a Robust Experimental Tool in High-Pressure Gas Turbine Combustion Tests. , 2014, , .		5
303	The influence of selected aromatic fluorescence tracers on the combustion kinetics of iso-octane. Fuel, 2019, 244, 559-568.	3.4	5
304	Studying the influence of single droplets on fuel/air ignition in a high-pressure shock tube. Review of Scientific Instruments, 2020, 91, 105107.	0.6	5
305	Kinetics of the Thermal Decomposition of Ethylsilane: Shock-Tube and Modeling Study. Energy & Fuels, 2021, 35, 3266-3282.	2.5	5
306	Flame Front Analysis in Turbulent Combustion. Informatik Aktuell, 2000, , 325-333.	0.4	5

#	Article	IF	CITATIONS
307	Shock-tube study of the influence of oxygenated additives on benzene pyrolysis: Measurement of optical densities, soot inception times and comparison with simulations. Combustion and Flame, 2022, 243, 111985.	2.8	5
308	Fiber optic spark plug sensor for UV-LIF measurements close to the ignition spark. , 2005, , .		4
309	On the effect of molecular and hydrocarbon-bonded hydrogen on carbon particle formation in C3O2 pyrolysis behind shock waves. Combustion and Flame, 2012, 159, 932-939.	2.8	4
310	Visualization of the gas flow in fuel cell bipolar plates using molecular flow seeding and micro-particle image velocimetry. Experiments in Fluids, 2012, 52, 743-748.	1.1	4
311	Investigation of the Mixing Process and the Fuel Mass Concentration Fields for a Gasoline Direct-Injection Spray at ECN Spray G Conditions and Variants. , 0, , .		4
312	Evaluation of Drude parameters for liquid Germanium nanoparticles through aerosol-based line-of-sight attenuation measurements. Journal of Quantitative Spectroscopy and Radiative Transfer, 2019, 226, 146-156.	1.1	4
313	Structures of carbonaceous nanoparticles formed in various pyrolysis systems. Carbon, 2019, 150, 244-258.	5.4	4
314	Structure–activity correlation in aerobic cyclohexene oxidation and peroxide decomposition over Co _{<i>x</i>} Fe _{3â^'<i>x</i>} O ₄ spinel oxides. Catalysis Science and Technology, 2022, 12, 3594-3605.	2.1	4
315	NO Laser-Induced Fluorescence Imaging in the Combustion Chamber of a Spray-Guided Direct-Injection Gasoline Engine. , 0, , .		3
316	Role of Non-Stationary Collisional Dynamics in Determining Nitric Oxide LIF Spectra. , 2004, , .		3
317	Laser-based imaging measurements in combustion: New results for fuel/air mixture and temperature diagnostics. Journal of Physics: Conference Series, 2006, 45, 27-27.	0.3	3
318	Toluene Laser-Induced Fluorescence (LIF) Imaging of Supersonic Flow within a Diverging Duct. , 2012, , 509-514.		3
319	Low temperature diffusion of Li atoms into Si nanoparticles and surfaces. Journal of Applied Physics, 2013, 114, 034310.	1.1	3
320	Ultraviolet absorption and laser-induced fluorescence of shock-heated acetylene. Proceedings of the Combustion Institute, 2017, 36, 4469-4475.	2.4	3
321	Temperature, pressure, and oxygen quenching behavior of fluorescence spectra and lifetimes of gas-phase o-xylene and 1,2,4-trimethylbenzene. Applied Physics B: Lasers and Optics, 2018, 124, 1.	1.1	3
322	Conflict-free railway track assignment at depots. Journal of Rail Transport Planning and Management, 2018, 8, 16-28.	0.8	3
323	Spontaneous-Raman-scattering measurements in diesel-like n-heptane jets: Spectroscopy and flame structure. Fuel, 2019, 236, 1356-1365.	3.4	3
324	Mixing processes in the transonic, accelerated wake of a central injector. Physics of Fluids, 2019, 31, .	1.6	3

#	Article	IF	CITATIONS
325	Low-temperature and low-pressure effective fluorescence lifetimes and spectra of gaseous anisole and toluene. Applied Physics B: Lasers and Optics, 2021, 127, 1.	1.1	3
326	Simultaneous measurement of liquid-film thickness and solute concentration of aqueous solutions of two urea derivatives using NIR absorption. Applied Optics, 2021, 60, 10087.	0.9	3
327	Shock tube study of the pyrolysis kinetics of Di- and trimethoxy methane. Combustion and Flame, 2022, 242, 112186.	2.8	3
328	Application of advanced laser diagnostics for the investigation of the ionization sensor signal in a combustion bomb. Applied Physics B: Lasers and Optics, 2005, 81, 1135-1142.	1.1	2
329	Effect of active impurities on the condensation of nanoparticles from supersaturated carbon vapor in the combined laser photolysis of C3O2 and H2S. Kinetics and Catalysis, 2008, 49, 167-177.	0.3	2
330	Enhanced long-term stability of functionalized silicon nanoparticles using esters. Materials Research Society Symposia Proceedings, 2009, 1207, 1.	0.1	2
331	Optical diagnostics in diesel combustion engines. , 2010, , 617-643.		2
332	Experimental Investigation of the Influence of the Pressure Gradient on the Transonic Mixing Behavior in Blunt-Body Wakes using Tracer LIF. , 2018, , .		2
333	Methodology for the investigation of ignition near hot surfaces in a high-pressure shock tube. Review of Scientific Instruments, 2018, 89, 055111.	0.6	2
334	Excitation wavelength dependence of the fluorescence lifetime of anisole. Physical Chemistry Chemical Physics, 2019, 21, 14562-14570.	1.3	2
335	Virtual Special Issue of Recent Advances in Gas-Phase Synthesis of Functional Materials for Energy. Energy & Fuels, 2021, 35, 6341-6343.	2.5	2
336	Survivability of the thermographic phosphors YAG:Pr and SMP:Sn in a premixed flame. Measurement Science and Technology, 2021, 32, 074001.	1.4	2
337	Direct rate-constant measurements and theoretical insight into the mechanism of the reactions H + hexamethyldisiloxane and H + tetramethyldisiloxane*. Molecular Physics, 0, , e1963871.	0.8	2
338	Thermochemistry of Oxygen-Containing Organosilane Radicals and Uncertainty Estimations of Organosilane Group-Additivity Values. Journal of Physical Chemistry A, 2021, 125, 8699-8711.	1.1	2
339	Temperature Diagnostics Using Laser-Induced Fluorescence (LIF) of Toluene. , 2006, , .		2
340	Spatially-resolved measurements of gas-phase temperature and SiO concentration in a low-pressure nanoparticle synthesis reactor using laser-induced fluorescence. , 2014, , .		2
341	In-cylinder thermographic PIV combined with phosphor thermometry using ZnO:Zn. International Journal of Engine Research, 2023, 24, 113-131.	1.4	2
342	Molecular Emissions from Stretched Excitation-Pulse in Nanosecond Phase-Selective Laser-Induced Breakdown Spectroscopy of TiO ₂ Nanoaerosols. Applied Spectroscopy, 2022, , 000370282110725.	1.2	2

#	Article	IF	CITATIONS
343	Strategies for NO Laser-Induced Fluorescence in Methane/Air Flames at Pressures between 1 and 60 bar. , 2002, , FB4.		1
344	Quantitative NO-LIF Temperature Imaging in High-Pressure Flames. , 2003, , .		1
345	Carbon Dioxide UV Laser-Induced Fluorescence Imaging in High-Pressure Flames. , 2004, , .		1
346	Recent Activities in Silicon Hydride Research in Europe. , 2011, , .		1
347	Application of Endoscopic OH*-Chemiluminescence Measurements at a Full-Scale High-Pressure Gas Turbine Combustion Test Rig. , 2012, , .		1
348	Synthesis of Tailored Nanoparticles in Flames: Chemical Kinetics, In Situ Diagnostics, Numerical Simulation, and Process Development. Nanoscience and Technology, 2012, , 3-48.	1.5	1
349	Experimental and Numerical Investigation of CH* and OH* Chemiluminescence in Acetylene Combustion behind Reflected Shock Waves. , 2012, , 421-426.		1
350	Measurements of Liquid Film Thickness and Solute Concentration of Aqueous NaCl Solution by Absorption Spectroscopy. , 2014, , .		1
351	Numerical Investigation of Transonic Mixing Behavior in the Wake of a Central Injector at different Reynolds numbers. , 2018, , .		1
352	Fuel effects on NO formation in diesel-like jets in a vessel. Combustion and Flame, 2019, 206, 201-210.	2.8	1
353	Toluene Laser-Induced Fluorescence (LIF) Imaging of Supersonic Flow within a Diverging Duct with Injectors in the Supersonic Region. , 2015, , 471-476.		1
354	Shock-tube study of the ignition delay time of tetraethoxysilane (TEOS). , 2009, , 781-785.		1
355	A Shock-Tube with High-Repetition-Rate Time-of-Flight Mass Spectrometry for the Study of Complex Reaction Systems. , 2012, , 191-196.		1
356	In-cylinder temperature measurements via fiber-based toluene-LIF time-correlated single-photon counting. , 2012, , .		1
357	UV-Absorption Measurements by Spontaneous Raman Scattering in Low-Sooting Diesel-Like Jets. , 0, , .		1
358	LASER-INDUCED INCANDESCENCE MEASUREMENTS OF SILICON AND COPPER NANOPARTICLES: SPECTROSCOPIC MODEL. , 2016, , .		1
359	Laser-induced atomic emission of silicon nanoparticles during synthesis in a microwave plasma reactor. , 2016, , .		1
360	A New Methodology to Study the Mechanisms of Combustion-Chamber Deposit Formation and the		1

Effects of Engine Parameters on the Quantity and Morphology of Combustion-Chamber Deposits. , 0, , .

#	Article	IF	CITATIONS
361	Intracavity Absorption Spectroscopy of CO2, CO and N2O Using a Fe:ZnSe Laser Tunable in the Range of 3.7–5.3 µm. , 2021, , .		1
362	A Compact Fiber-Coupled NIR/MIR Laser Absorption Instrument for the Simultaneous Measurement of Gas-Phase Temperature and CO, CO2, and H2O Concentration. Sensors, 2022, 22, 1286.	2.1	1
363	Application of laser diagnostics to engine combustion. , 0, , .		0
364	Laser-induced fluorescence detection of no in high-pressure flames with A-X(0,0), (0,1), and (0,2) excitation. , 2002, , .		0
365	Thickness imaging of evaporating liquid water films by simultaneous Tracer-LIF, Raman imaging and Diode Laser Absorption Spectroscopy. , 2012, , .		Ο
366	Selected papers about chemiluminescence of flames. Applied Physics B: Lasers and Optics, 2012, 107, 513-514.	1.1	0
367	In Situ Particle Size Measurements of Gas-Borne Silicon Nanoparticles by Time-Resolved Laser-Induced Incandescence. , 2013, , .		Ο
368	Laser-Induced Incandescence (LII) Measurements on Gas-Borne Silicon Nanoparticles. , 2014, , .		0
369	Liquid film thickness measurement by two-line TDLAS. , 2014, , .		Ο
370	Applications of Intracavity Absorption Spectroscopy to Quantitative Gas-Phase Species and Temperature Diagnostics. , 2016, , .		0
371	Transport and Diffusion in Boundary Layers of Turbulent Channel Flow. , 2007, , 419-432.		Ο
372	Micro-invasive LIF Diagnostics in Engines. , 2008, , .		0
373	Temperature dependence of the soot yield in shock wave pyrolysis of carbon-containing precursors. , 2009, , 183-188.		Ο
374	In-Situ Laser Diagnostics of Temperature, Intermediate Species Concentration and Particle Sizes in Gas-Phase Nanoparticle Synthesis. , 2010, , .		0
375	Measurements of Liquid Film Thickness by Tracer LIF, Raman Scattering and Diode Laser Absorption Spectroscopy. , 2010, , .		Ο
376	Functionalization of SiO2 Nanoparticles and Their Superhydrophobic Surface Coating. Special Publication - Royal Society of Chemistry, 2012, , 113-120.	0.0	0
377	High speed in-cylinder laser hygrometry for EGR quantification using a wavelength scanned vertical cavity surface emitting laser. , 2012, , .		0
378	In Situ Laser Diagnostics in the Gas-Phase Synthesis of Functional Nanomaterials. , 2014, , .		0

#	Article	IF	CITATIONS
379	Analysis of Chemical Dynamics and Technical Combustion by Time-Resolved Laser-Induced Fluorescence. , 1999, , 241-275.		0
380	DLAS-based measurement of water film thickness in retro-reflection. , 2016, , .		0
381	Water Film Thickness Imaging based on Time-Multiplexed Near-Infrared Absorption. , 2018, , .		0
382	Strategy for determining absolute concentration levels of SiO in low pressure gas phase synthesis flames for silica nanoparticles. , 2018, , .		0
383	Characterization of Oxygenated-Fuel Combustion by Quantitative Multiscalar SRS/LIF Measurements in a Diesel-Like Jet. , 0, , .		0
384	Characterization of tracers for two-color laser-induced fluorescence liquid-phase temperature imaging in sprays. , 2020, , .		0